A Hybrid Dynamic Nonlinear Controller For Variable Speed Wind Turbine In Low Wind Velocity Regime

EL Kabira EL MJABBER[1], *Abdellatif KHAMLICHI*[1]

[1]Team 3M, Department of Industrial and Civil Sciences and Technologies, National School of Applied Sciences, University Abdelmalek Essaadi, Street Sebta, Tetouan, Morocco

kabira.mjabber@gmail.com, akhamlichi@uae.ac.ma

DOI: 10.15598/aeee.v22i2.5335

Article history: Received Jul 27, 2023; Revised Dec 17, 2023; Accepted Apr 22, 2024; Published Jun 30, 2024.

Abstract. *The purpose of this paper is to propose a new control approach to be applied to a variable rotor speed wind turbine at a low wind velocity zone. The aim is to reduce dynamic mechanical loads and optimize energy production by acting on the generator torque through a new hybrid adaptive controller. This combines two well-known nonlinear methods: nonlinear control based on Radial Basis Function Neural Networks used to estimate the nonlinear part of the wind turbine system and Integral Sliding Mode Control to tackle system uncertainties. Lyapunov's approach has been applied to assess the stability of this new controller. Then, simulations were carried out using the Matlab/Simulink software package. The obtained results demonstrated the superior performance of the hybrid controller compared to each controller taken alone.*

Keywords

Nonlinear control, integral sliding mode control, radial basis function neural network controller, variable speed wind turbine control, wind energy.

1. Introduction

Wind energy is a renewable clean energy that has become competitive nowadays due to various technological advances that have been achieved these recent years. Optimization of energy capture from wind still suffers from obstacles such as the stochastic nature of wind speed. These cause continuous fluctuations that impede tracking the optimal rotor speed without causing variations of mechanical loads acting on key parts of the wind turbine installation, such as torque in the transmission line. So, the controllers are required to ensure a safe and efficient conversion of kinetic energy contained in wind into electricity while dealing with the presence of these sources of disturbances. Otherwise, these may deteriorate energy quality and reduce the life of equipment due to accelerated fatigue [1].

Numerous approaches to controlling wind turbines have been proposed in the literature, including both linear and nonlinear methods [2–5]. Since wind turbines are nonlinear systems, conventional linear controllers are known to lack robustness and can only remain stable within a limited operating range [3] and [6]. Consequently, there is a growing interest in employing nonlinear control laws, which can better adapt to variations in system parameters and environmental conditions. As a result, several nonlinear control strategies have been introduced. Notably, the works cited in [6] and [7] represent significant approaches in the literature.

New perspectives have emerged recently in the field of nonlinear control with the apparition of intelligent adaptive controllers. The best-known methods in this field are controllers based on neural networks [8], fuzzy logic [9], and Radial Basis Function Neural Networks (RBF-NN) which are mostly used to adjust Proportional Integral (PI) gains and to perform dynamic neural approximation [10–12].

The Sliding Mode Control (SMC) is particularly suitable for wind turbines because of its robust be-

havior under uncertainties that can affect the system [13–15]. The researchers have used SMC-based controllers to maximize the capture of wind energy while reducing load fluctuations on the drive train to limit the fatigue loads [1] and [16].

SMC is recognized for its drawback of frequent switching between various control values, leading to a chattering phenomenon that induces increased mechanical stress on system components. To alleviate this issue, researchers have introduced several techniques to mitigate chattering effects [17]. Capitalizing on the inherent robustness of SMC, a derivative technique, the Super Twisting Algorithm (STA), has been amalgamated with other approaches. Authors in [18] utilized STA to alleviate the chattering problem. The integration of STA with SMC, denoted as STA-SMC, employing Space Vector Modulation (SVM), has been employed by [19] for the control of the Double Fed Induction Generator (DFIG).

The effectiveness of SMC-based Artificial Neural Networks (ANN) has been demonstrated in various studies. For instance, [20] applied an SMC-based ANN to regulate the active and reactive power of DFIG. Additionally, the STA-based ANN proposed by [21] has been utilized to control a floating wind turbine in Region III.

The existing literature extensively covers various control strategies for wind turbine systems aimed at optimizing energy production and reducing mechanical loads. However, there is a clear need for further research into integrating nonlinear control methods, specifically combining RBF-NN for nonlinear system estimation and ISMC for managing system uncertainties. While individual studies have examined these methods separately, there is limited research on this joint application of wind turbine control, especially in maximizing energy by considering the mechanical part modeled by two masses. Additionally, there is a lack of thorough analysis regarding the proposed hybrid adaptive controller using the Lyapunov approach. Addressing these research gaps is crucial for advancing our understanding of effective control strategies in wind energy systems and enhancing their performance under dynamic conditions.

Contribution of this paper:
This paper focuses on a variable-speed wind turbine operating at low wind speeds (below-rated speed) and presents the following contributions:

- An intelligent hybrid nonlinear controller: The paper proposed a controller that combines the use of RBF-NN to estimate the uncertain variables in the wind turbine system and Integral Sliding Mode Control ISMC protocol to track the optimal rotor speed. This hybrid controller aims to address the chattering phenomenon typically associated with conventional SMC-based controllers while compensating for the lack of an accurate wind turbine model through RBF-NN training. The goal is to synergistically leverage the strengths of both controllers to enhance the robust behavior of the ISMC strategy.
- Maximizing wind energy extraction: The proposed control strategy aims to maximize the extraction of wind energy by following the optimal Tip Speed Ratio (TSR). By optimizing the rotor speed based on TSR, the controller seeks to achieve optimal energy capture from the wind.
- Minimizing mechanical load fluctuations: Another objective of the proposed controller is to minimize fluctuations that affect mechanical loads to enhance the lifetime of the wind turbine system. By regulating the electromagnetic torque, the controller aims to minimize control errors while tracking the optimal rotor speed.

In summary, the paper introduces an intelligent hybrid nonlinear controller that combines RBF-NN and ISMC techniques. The controller aims to improve the robustness of the ISMC strategy, maximize mechanical load fluctuations to enhance the longevity of the wind turbine system .

2. Wind turbine modeling

Wind turbines with horizontal rotor axes are nowadays widely used [22]. Often for control purposes, a simplified mechanical model of such a complex system is considered [23, 24]. The aerodynamic power extracted by a wind turbine can be expressed as:

$$P_a = \frac{1}{2}\rho\pi R^2 C_p v^3, \tag{1}$$

where ρ denotes air density in (kg.m^{-3}), R represents the radius of the wind turbine in (m), v is the average wind speed in (m.s^{-1}) at the rotor level, and C_p the power coefficient. This last is a characteristic factor specific to a particular wind turbine. It represents its ability to extract energy from the kinetic energy present in the wind. This coefficient varies depending on the design of the wind turbine blades and the operating conditions. It can be determined through experimental testing or estimated using numerical simulations and computational models. For the specific wind turbine chosen in this study, C_p can be approximated using the following equation [25]:

$$\begin{aligned} C_p(\lambda,\beta) &= c_1\left(c_2\chi - c_3\beta - c_4\right)e^{-c_5\chi} + c_6\lambda \\ \chi &= \frac{1}{\lambda + 0.08\beta} - \frac{0.035}{\beta^3+1}, \end{aligned} \tag{2}$$

in which the constants $c_1, c_2, c_3, c_4, c_5, c_6$ depend on the given wind turbine, β is the pitching angle of the wind turbine blades in ($\circ$) and λ is the tip speed ratio. This last parameter is defined as the ratio of the linear velocity at the tip of the blades divided by the wind speed. It is written as:

$$\lambda = \frac{\omega_t}{v} R, \tag{3}$$

where ω_t is the rotational speed at which the rotor turns actually. This speed is typically measured and expressed in revolutions per minute (rpm).

Fig. 1 presents a three-dimensional representation of the power coefficient for the specific wind turbine considered in this work. This figure illustrates that the power coefficient reaches a maximum value for an optimal pitch $\beta = \beta_{opt}$ and an optimal tip-speed ratio $\lambda = \lambda_{opt} = 7.5$.

The aerodynamic torque is obtained by dividing the aerodynamic power, as defined in Eq. (1), by the rotor speed ω_t:

$$T_a = \frac{P_a}{\omega_t} = \frac{\rho \pi R^2}{2} \frac{C_p(\lambda, \beta) v^3}{\omega_t}. \tag{4}$$

In general, the drive train of a wind turbine consists of several components, including a generator, a gearbox, a rotor, a high-speed shaft and a low-speed shaft. This mechanical system can be represented roughly by a rigid one degree of freedom system in which the whole inertia of turning parts is integrated. However, a refined model that gives more insight into the transmission line dynamics has been introduced by taking into account the flexibility of the primary shaft. The resulting wind turbine model takes then the form of an equivalent discrete two-mass model representing the inertia of the turbine rotor and the power train. The schematic representation of this two degrees of freedom system is depicted in Fig. 2.

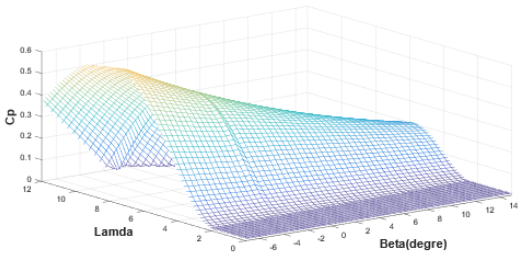

Fig. 1: 3D representation of the power coefficient as function of blades pitch angle β and tip speed ratio λ.

In Fig. 2, K_{ls}, K_r, K_g denote the external damping, B_{ls} is the low-speed shaft stiffness, T_{ls} and T_{hs} are respectively the low and high-speed shaft torques, T_{em} represents the electromagnetic torque, ω_g is the generator speed, and J_r and J_g are the rotor and generator inertia respectively.

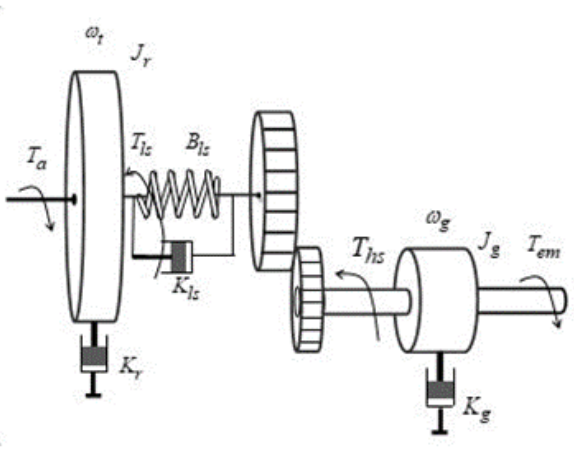

Fig. 2: Equivalent wind turbine model with two masses.

The dynamic equation of the inertia in the rotor side J_r in (kg.m2) expresses the evolution of the rotor speed ω_t under the action of the aerodynamic torque T_a in (Nm), the torque exerted on the gearbox extremity linked to slow speed shaft, denoted T_{ls}, and a viscous frictional torque $K_r\omega_t$. This equation takes the form [22]:

$$\dot{\omega}_t = \frac{T_a}{J_r} - \frac{T_{ls}}{J_r} - \frac{K_r}{J_r}\omega_t. \tag{5}$$

The dynamic of the inertia on the generator side J_g in (kg.m^2) describes the time variation of generator shaft speed resulting from the application of the torque T_{hs} on the gearbox side, as well as the torque T_{em} and a viscous frictional torque $K_g\omega_g$.This equation writes [12]:

$$\dot{\omega}_g = \frac{T_{hs}}{J_g} - \frac{K_g}{J_g}\omega_g - \frac{T_{em}}{J_g}. \tag{6}$$

The torques T_{ls} and T_{hs} vary inversely with the speeds ω_t and ω_g since:

$$n_g = \frac{T_{ls}}{T_{hs}} = \frac{\omega_g}{\omega_t} = \frac{\theta_g}{\theta_t}, \tag{7}$$

where n_g is the gearbox ratio

The elastic behavior of the slow-speed shaft, coupled with the absence of external loading between its extremities [26], allows for the torque it experiences on the gearbox side T_{ls} to be related to the elastic and frictional effects by:

$$T_{ls} = B_{ls}(\theta_t - \theta_{ls}) + K_{ls}(\omega_t - \omega_{ls}). \tag{8}$$

Using $\omega_{ls} = \omega_g/n_g$ and $T_{hs} = T_{ls}/n_g$, and substituting (5) and (6) into the expression of the time deriva-

tive of Eq. (8), one gets:

$$\dot{T}_{ls} = \left(B_{ls} - \frac{K_{ls}K_r}{J_r}\right)\omega_t + \frac{1}{n_g}\left(\frac{K_{ls}K_g}{J_g} - B_{ls}\right)\omega_g + K_{ls}\left(\frac{T_a}{J_r} + \frac{T_{em}}{n_g J_g}\right) - K_{ls}T_{ls}\left(\frac{J_r + n_g^2 J_g}{n_g^2 J_r J_g}\right). \quad (9)$$

The global state system, Eq. (10), which describes the dynamics of the two masses wind turbine model, is deduced from (5), (6), and (9).

3. Wind turbine control

3.1. Design of integral sliding mode control ISMC

SMC is well suited for controlling nonlinear and uncertain equilibrium trajectories and enhance control stability [27]:

$$S(t) = \delta\, e + \frac{de}{dt} + G_i \int e(t)dt, \quad (11)$$

where δ represents positive gain and G_i is the integral gain.

The control error (tracking error) is defined by the optimum rotor speed ω_{opt} and rotor speed ω_t as:

$$e = \omega_{opt} - \omega_t. \quad (12)$$

The optimum rotor speed expression can be obtained from Eq. (3) as follows:

$$\omega_{opt} = \frac{\lambda_{opt} v}{R}. \quad (13)$$

The control input denoted u should ensure local attractiveness to surface S in its vicinity, i.e., the system trajectory (11) must be directed towards it and intersect it. For this purpose, a sufficient stability condition of $S(x,t) = 0$, called the attractiveness condition, has to be satisfied by the controller. In the context of the direct Lyapunov method, an unbounded function $V(S)$ called the Lyapunov function should be exhibited with $V(0) = 0$ and $V(\infty) = \infty$. Its time derivative $\frac{dV}{dt}$ provides information on the stability of the system, such that if $\frac{dV}{dt} < 0$ for $S \neq 0$ then the system is asymptotically stable.

One of the simplest Lyapunov functions that can be proposed in the context of ISMC is the classical quadratic systems. ISMC enhances SMC by integrating integral action, providing improved tracking accuracy and disturbance rejection compared to standard SMC. In the context of modeling wind turbines with a two-mass system and enhancing control stability, incorporating integral action into the expression of the sliding surface is essential. This refined surface formulation aims to better describe function:

$$V(S) = \frac{1}{2}S(x,t)^2. \quad (14)$$

The function $V(S)$ is positive. Then, it is sufficient to impose its time derivative to be negative to ensure convergence of S towards zero. This condition writes

$$\frac{dV(S)}{dt} = S(x,t)\frac{dS(x,t)}{dt} \leqslant 0. \quad (15)$$

In this study, the Lyapunov function is chosen to be defined by Eq. (14) to ensure the stability of the system through condition (15). Forcing the quantity $S(x,t)^2$ to decrease all the time serves to force the trajectory of the system towards the sliding surface. In this case it is of course assumed that the switching frequency is infinite. The ideal sliding regime is obtained by using the time derivative of Eq. (11) and subsituting it into Eq. (15) under the following form:

$$S\left[\delta\left(\frac{d\omega_{opt}}{dt} - \frac{d\omega_t}{dt}\right) + \frac{d^2e}{dt^2}\right] \leqslant 0. \quad (16)$$

ISMC control law:
Considering the time derivative of the sliding surface as defined by Eq. (11) along with Eq. (12) gives:

$$\frac{dS}{dt} = \delta\frac{de}{dt} + \frac{d^2e}{dt} + G_i e = \delta\left[\frac{d\omega_{opt}}{dt} - \frac{d\omega_t}{dt}\right] + \frac{d^2e}{dt} + G_i e. \quad (17)$$

Using now equations (5), (6) and (7), the low speed shaft torque can be put under the following form:

$$T_{ls} = n_g J_g \dot{\omega}_g + K_g n_g \omega_g + n_g T_{em}. \quad (18)$$

Using Eqs. (6) and (18), the rotor dynamics under the action of T_{em} is obtained as:

$$\frac{d\omega_t}{dt} = \frac{T_a}{J_r} - \frac{K_r}{J_r}\omega_t - \frac{n_g J_g}{J_r}\frac{d\omega_g}{dt} - \frac{n_g K_g}{J_r}\omega_g - \frac{n_g}{J_r}T_{em}. \quad (19)$$

To apply ISMC, Eq. (19) must be rewritten under the general nonlinear control form as:

$$\frac{d\omega_t}{dt} = f(\omega_t, \omega_g) + gT_{em}, \quad (20)$$

with $f(\omega_t,\omega_g) = \frac{T_a}{J_r} - \frac{K_r}{J_r}\omega_t - \frac{n_g J_g}{J_r}\frac{d\omega_g}{dt} - \frac{n_g K_g}{J_r}\omega_g$ and $g = -\frac{n_g}{J_r}$.

$$\begin{bmatrix}\dot{\omega}_t\\ \dot{\omega}_g\\ \dot{T}_{ls}\end{bmatrix}=\begin{bmatrix}-K_r/J_r & 0 & -1/J_r\\ 0 & -K_g/J_g & 1/[n_gJ_g]\\ B_{ls}-\frac{K_{ls}K_r}{J_r} & \frac{1}{n_g}\left(\frac{K_{ls}K_g}{J_g}-B_{ls}\right) & -K_{ls}\left(\frac{J_r+n_g^2J_g}{n_g^2J_gJ_r}\right)\end{bmatrix}\begin{bmatrix}\omega_t\\ \omega_g\\ T_{ls}\end{bmatrix}+\begin{bmatrix}1/J_r\\ 0\\ K_{ls}/J_r\end{bmatrix}T_a+\begin{bmatrix}0\\ -1/J_g\\ K_{ls}/[n_gJ_g]\end{bmatrix}T_{em}. \tag{10}$$

The control input u consists of two terms. The equivalent term $u_{eq}=T_{em}$ is utilized to control system variations, meaning that it provides the tracking reference for the system. On the other hand, the robustness term u_r is used to force the system to vary on the sliding surface.

$$u=u_{eq}+u_r. \tag{21}$$

By subsituting $\dot{\omega}_t$ obtained from Eq. (20) into Eq. (17) with imposing $\dot{S}=0$, the expression of u_{eq} is then found as follows:

$$u_{eq}=\frac{1}{g}\left(-f(\omega_t,\omega_g)+\frac{1}{\delta}\frac{de^2}{dt}+\frac{G}{\delta}e+\frac{\omega_{opt}}{v}\frac{dv}{dt}\right). \tag{22}$$

To minimize the interference phenomenon, the hyperbolic tangent function (tanh) is used to obtain a smooth control law under the form:

$$u_r=\eta\tanh(S), \tag{23}$$

where the constant η represents the switching gain.

By using Eqs. (21), (22) and (23), the global law of the control is deduced as:

$$u=\frac{1}{g}\left(-f(\omega_t,\omega_g)+\frac{1}{\delta}\frac{de^2}{dt}+\frac{G}{\delta}e+\frac{\omega_{opt}}{v}\frac{dv}{dt}\right)+\eta\tanh \tag{24}$$

3.2. Design of nonlinear controller RBF-NN

RBF-NN offers several advantages such as the fact that its local behavior is very intuitive. RBF-NN admits a single hidden layer which makes it easier to use and faster than conventional multilayer perceptron structure. RBF-NN has gained interest for its universal faculty of computation, estimation and control of uncertain systems. RBF, Fig. 3, consists of three layers, an input layer that contains the input variables x_i, a hidden layer that is activated by radial basis function ψ_j and an output layer f. Taking into account the approximate network error, the output of an RBF-NN is written as [28]:

$$f(\omega_t)=W^T\Psi(e)+\nu, \tag{25}$$

where $\Psi(e)=[\psi_1,\ \psi_2,\ ...,\ \psi_p]$ is a radial function vector, W^T is the vector of optimal weights, and v is the uncertainty that can be assumed to be bounded by $\nu_{\max}$: $|\nu|<\nu_{\max}$.

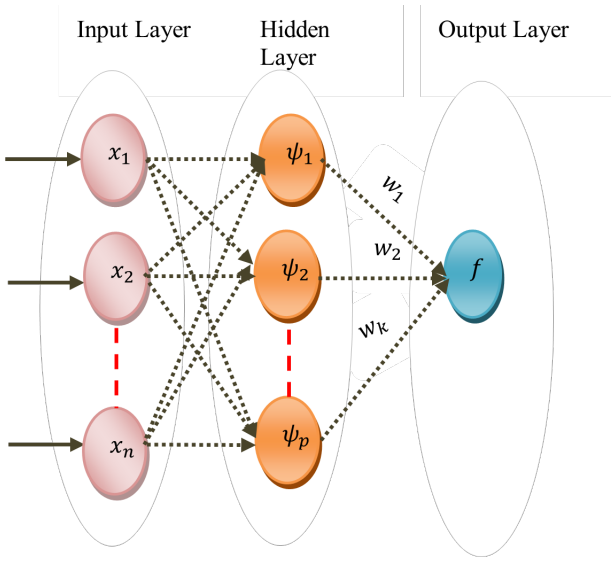

Fig. 3: RBF network architecture.

The optimal weighs are solutions to an optimization problem which has the form [29]:

$$W=\arg\min\left[\sup\left|\hat{f}(X)-f(X)\right|\right]. \tag{26}$$

To produce the output of the hidden layer, the following nonlinear activation function is used [29]:

$$\psi_j(e)=\exp\left(-\frac{\|e-C_j\|^2}{2\sigma_j^2}\right), \tag{27}$$

where C_j represents the center of Gaussian function ψ_j and σ_j the width of each ψ_j.

RBF-NN Control law:
To extract the control law $u=T_{em}$, the second order dynamic is imposed on the tracking error as stated by Eq. (12):

$$\frac{d^2e(t)}{dt}+k_1\frac{de}{dt}+k_2e=0, \tag{28}$$

with k_1 and k_2 being two positive scalars, chosen so that $s^2+k_1s+k_2$ polynomial is Hurwitz. In order to ensure stability of the equilibrium, $\frac{de}{dt}$ is substituted by

the time derivative of the right-hand side of Eq. (12), which leads to:

$$\frac{d^2e(t)}{dt} + k_1\left(\frac{d\omega_{opt}}{dt} - \frac{d\omega_t}{dt}\right) + k_2 e = 0. \tag{29}$$

Replacing the $\frac{d\omega_t}{dt}$ in Eq. (29) with the expression from Eq. (20), the control law becomes as follows:

$$\begin{cases} u_{eq} = \dfrac{1}{g}\left(-f(\omega_t,\omega_g) + \dfrac{1}{k_1}\dfrac{de^2}{dt} + \dfrac{k_2}{k_1}e + \dfrac{\omega_{opt}}{v}\dfrac{dv}{dt}\right) \\ f(\omega_t,\omega_g) = \dfrac{T_a}{J_r} - \dfrac{K_r}{J_r}\omega_t - \dfrac{n_g J_g}{J_r}\dot{\omega}_g - \dfrac{n_g K_g}{J_r}\omega_g \end{cases}. \tag{30}$$

Applying the control law of the ISMC as given by Eq. (24), and imposing the dynamic to the error of speed to be that given in Eq. (28), the global ISMC control law writes:

$$\begin{cases} u = \dfrac{1}{g}\left(-f(\omega_t,\omega_g) + \dfrac{1}{k_1}\dfrac{de^2}{dt} + \dfrac{k_2}{k_1}e + \dfrac{\omega_{opt}}{v}\dfrac{dv}{dt}\right) \\ +\eta\tanh(S) \\ f(\omega_t,\omega_g) = \dfrac{T_a}{J_r} - \dfrac{K_r}{J_r}\omega_t - \dfrac{n_g J_g}{J_r}\dfrac{d\omega_g}{dt} - \dfrac{n_g K_g}{J_r}\omega_g \end{cases}. \tag{31}$$

As $f(\omega_t,\omega_g)$ is highly nonlinear which may affect the control reliability, estimating this function by an RBFNN allows for a more accurate representation of the system. The estimation is considered under the form:

$$\hat{f}(e) = \hat{W}^T\Psi(e). \tag{32}$$

The RBFNN control law developed of the two-masses wind system is given by:

$$\begin{cases} \hat{u} = \dfrac{1}{g}\left(-\hat{f}(e) + \dfrac{1}{k_1}\dfrac{d^2e}{dt} + \dfrac{k_2}{k_1}e + \dfrac{\omega_{opt}}{v}\dfrac{dv}{dt}\right) \\ \hat{f}(e) = \hat{W}^T\psi(e) \end{cases}. \tag{33}$$

The weights $\hat{W}$ can be updated using the following rule:

$$\dot{W} = -\varsigma\hat{f}\,e + \chi|e|\,\hat{W}, \tag{34}$$

where $\varsigma > 0$ and $\chi > 0$.

3.3. Hybrid control ISMC-RBF:

The ISMC controller, as described in Eq. (30), often exhibits a chattering phenomenon, which can have detrimental effects on the power quality and the mechanical and electrical components of the wind turbine. Given the nonlinear nature of wind turbine systems, the accuracy of uncertain components is crucial. Integrating an RBF-NN representation of these nonlinearities is expected to be beneficial in mitigating this ISMC perturbations.

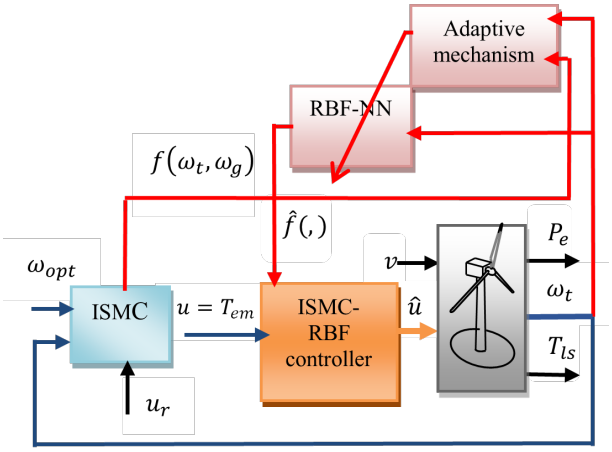

Fig. 4: Block scheme of the hybrid proposed controller ISMC-RBF.

Our proposed method aims to address the chattering phenomenon while retaining the advantages of the sliding control mode approach. The ISMP component introduces integral action, effectively eliminating steady-state errors and reducing the impact of high-frequency oscillations. Simultaneously, the incorporation of RBF helps to smooth the control signal transitions, providing a more continuous and stable response. Together, these elements synergistically address the chattering phenomenon inherent in the traditional sliding mode techniques.

This yields a new hybrid controller that combines both ISMC and RBF-NN methods which constitutes the main contribution of this work, (see Fig. 4).

Using the estimation $f(\omega_t,\omega_g)$ as given in Eq. (33), instead of the explicit expression given in Eq. (31), the hybrid control law writes as follows:

$$\begin{cases} u = \dfrac{1}{g}\left(-f(\omega_t,\omega_g) + \dfrac{1}{k_1}\dfrac{de^2}{dt} + \dfrac{k_2}{k_1}e + \dfrac{\omega_{opt}}{v}\dfrac{dv}{dt}\right) \\ +\eta\tanh(S) \\ \hat{f}(e) = \hat{W}^T\psi(e) \end{cases}. \tag{35}$$

In addition to system nonlinearities, a disturbance d is assumed to disrupt the dynamics of the wind turbine. The system dynamic equation in terms of the rotor speed, Eq. (20), is then modified according to:

$$d\omega_t/dt = f(\omega_t) + gu + d, \tag{36}$$

in which the disturbance is considered to be bounded such that $|d| \leqslant D$.

Stability study is essential for any system control. In this work, considering the dynamic and non-linear nature of the proposed controller presented by Eq. (35), Lyapunov's theorem was chosen to ensure the stability of the learning algorithm, as follows:

$$d\hat{W}\Big/dt = -\left(1/\gamma\right)e\Psi\left(e\right), \quad \gamma > 0, \tag{37}$$

Proof of stability for the hybrid controller ISMC-RBF

Take the Lyapunov function to be:

$$V = \frac{1}{2}\gamma\bar{W}^T\bar{W} + \frac{1}{2}e^2, \tag{38}$$

with $\bar{W} = W - \hat{W}$ and $\gamma > 0$. Taking the time derivative of Eq. (38), one gets:

$$\begin{aligned}\frac{dV}{dt} &= \frac{1}{2}\gamma\left(\frac{d\bar{W}}{dt}\right)^T\bar{W} + \frac{1}{2}\gamma\bar{W}^T\left(\frac{d\bar{W}}{dt}\right) + e\frac{de}{dt} \\ &= \gamma\bar{W}^T\left[\frac{dW}{dt} - \frac{d\bar{W}}{dt}\right] + e\frac{de}{dt}.\end{aligned} \tag{39}$$

The stationary property of is derived from its state of optimality and can be expressed as follows:

$$\frac{dW}{dt} = 0. \tag{40}$$

Substituting Eq. (40) into Eq. (39), yields:

$$\frac{dV}{dt} = -\gamma\bar{W}^T\left(\frac{d\hat{W}}{dt}\right) + e\frac{de}{dt}. \tag{41}$$

By using Eqs. (15) and (36), Eq. (41) can be simplified as:

$$\frac{dV}{dt} = -\gamma\bar{W}^T\left(\frac{d\hat{W}}{dt}\right) + e\left(\frac{d\omega_{opt}}{dt} - f - gu - d\right). \tag{42}$$

By substituting Eq. (36) into Eq. (42), the derivative of the Lyapunov function can be expressed as follows:

$$\begin{aligned}\frac{dV}{dt} &= e\left[-f + \hat{f} - \frac{1}{k_1}\left(\frac{de^2}{dt}\right) - \frac{k_2}{k_1}e - \eta g\tanh(S) - d\right] \\ &\quad - \gamma\bar{W}^T\left(\frac{d\hat{W}}{dt}\right).\end{aligned} \tag{43}$$

The optimization error can be denoted by:

$$\bar{f} = f - \hat{f}. \tag{44}$$

By utilizing equations Eqs. (25) and (32), it is possible to express this error in the following manner:

$$\bar{f} = \bar{W}\Psi + \nu. \tag{45}$$

Substituting (45) into (42), one obtains after some obvious algebraic calculation:

$$\begin{aligned}\frac{dV}{dt} &= -e\left[\frac{1}{k_1}\left(\frac{de^2}{dt}\right) + \frac{k_2}{k_1}e + \eta g\tanh(S) + \nu + d\right] \\ &\quad \bar{W}^T\left[-\gamma\left(\frac{d\hat{W}}{dt}\right) - e\Psi\right].\end{aligned} \tag{46}$$

Considering the dynamics of the weight estimates according to the learning algorithm given by Eq. (37), then the Lyapunov function derivative given in Eq. (46) becomes:

$$\frac{dV}{dt} = -\frac{1}{\delta}\left(e\frac{de^2}{dt}\right) - e\left[\nu + d + \frac{k_2}{k_1}e + \eta g\tanh(S)\right]. \tag{47}$$

We can now easily see that for $v, d \to 0$ the condition of stability to be met has the obvious following form:

$$\frac{dV}{dt} = -\frac{1}{k_1}\left(e\frac{de^2}{dt}\right) - \frac{k_2}{k_1}e^2 - e\eta g\tanh(S) \leqslant 0. \tag{48}$$

4. Results and discussion

In this study, the performance of the developed control approach is evaluated through numerical simulations conducted on the Controls Advanced Research Turbine (CART) [3]. CART has been specifically designed to facilitate the investigation and research of control tests for large-scale turbines. This variable-speed wind turbine is equipped with a flexible hub, variable pitch mechanism, and two blades, each driven independently by its electromechanical system, allowing for individual pitching control. The nominal power output of CART is 600 kW. The other characteristics of this turbine are presented in Appendix A.

To assess efficiency of the hybrid controller, various parameters are taken into consideration across different mean wind speeds. These include:

- Tracking of optimal rotor speed: This involves minimizing tracking errors to ensure the rotor speed closely follows the desired trajectory.
- Maximum electromagnetic torque (Max (Tem)): This parameter determines the maximum torque exerted on the turbine generator, providing insights into mechanical loading.
- Maximum electrical power (Max (Pe)): This represents the highest level of power output generated by the wind turbine electrical system.
- Standard Deviation (STD) of electrical power: The STD indicates the variability or fluctuation in electrical power output, providing information on the stability of power generation.

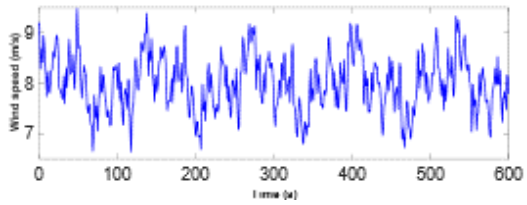

Fig. 5: Wind velocity profile with mean value = 8 m.s^{-1}.

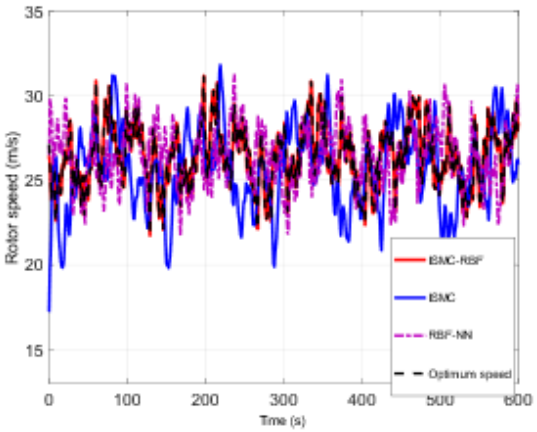

Fig. 6: The time response of the rotor speed.

- Efficiency (η_{el}): Efficiency measures how effectively the controller converts available wind energy into usable electrical power, typically represented as the ratio of electrical power output to the available wind power.

$$\eta_{el}(\%) = \frac{\int_{t_i}^{t_f} P_e dt}{\int_{t_i}^{t_f} P_{a,opt} dt}. \tag{49}$$

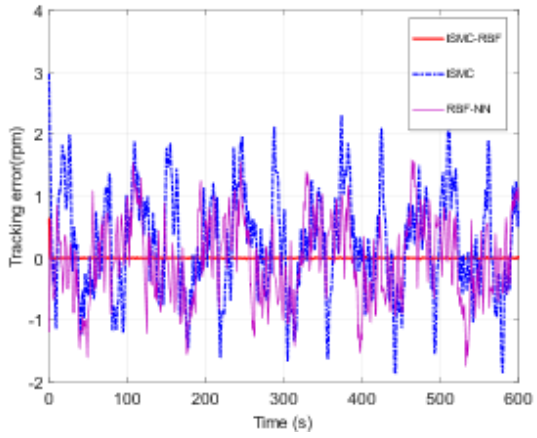

Fig. 7: The time response of the tracking error.

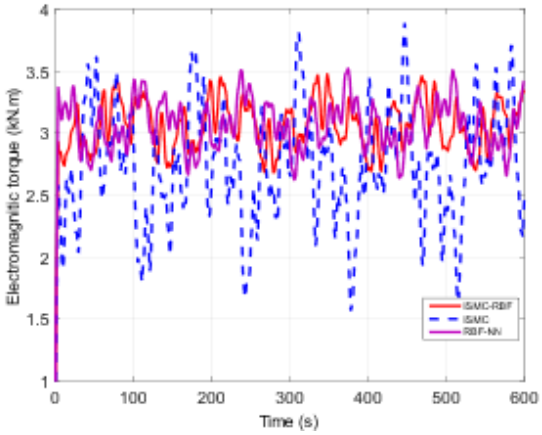

Fig. 8: The time response of the electromagnetic torque.

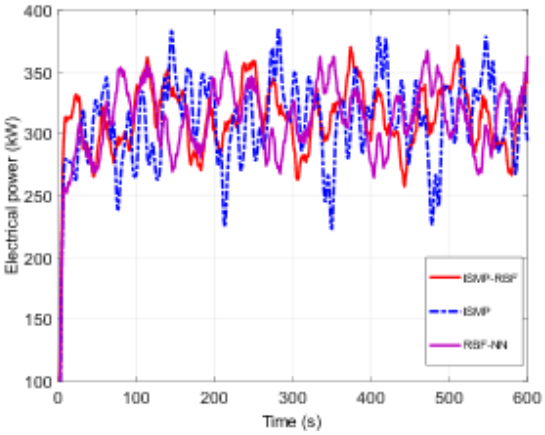

Fig. 9: The time response of the electrical power.

where t_f and t_i are the considered limits of the time interval. P_e is the actual power extracted and $P_{a,opt}$ is the optimal aerodynamic power which is given by:

$$P_{a,opt} = 0.5\rho\pi R^2 C_{p,\max} v^3. \tag{50}$$

Assessing these parameters across different mean wind speeds provides valuable insights into the hybrid controller performance and its ability to adapt to varying environmental conditions.

The variations in wind speed are modeled to range between 7 and 9 m.s^{-1}, representing 50% of the standard of the deviation wind spectrum. Fig. 5 illustrates the wind data used in the simulation, with a mean wind speed of 8 m.s^{-1}.

A comparison among three control techniques, RBF-NN, ISMC, and ISMC-RBF, is conducted to ascertain the most effective method and highlight the advantages of combining different control techniques. The analysis of results from the three controllers, as depicted in Fig. 6, indicates that ISMC alone struggles to accurately track the optimal rotor speed. However, the

Tab. 1: Benchmarking performance of the 3 controllers with mean speed= 7m/s.

7 m/s	η_{el}	**Max** (P_e)	**Max** (T_{em})	**STD** (T_{em})
ISMC	90.2%	350	1.97	0.245
NN-RBF	93%	296	1.50	0.120
ISMC-RBF	95.5%	290	1.21	0.022

Tab. 2: Benchmarking performance of the 3 controllers with mean speed= 8m/s.

8 m/s	η_{el}	**Max** (P_e)	**Max** (T_{em})	**STD** (T_{em})
ISMC	85%	385	3.88	0.474
NN-RBF	93%	296	1.50	0.227
ISMC-RBF	95.5%	290	1.21	0.220

Tab. 3: Benchmarking performance of the 3 controllers with mean speed= 9m/s.

9 m/s	η_{el}	**Max** (P_e)	**Max** (T_{em})	**STD** (T_{em})
ISMC	74%	610	4.10	0.510
NN-RBF	78.8 %	454	3.99	0.254
ISMC-RBF	79%	450	3.80	0.240

hybrid technique ISMC-RBF yields satisfactory results compared to the other two methods. Moreover, the presence of disturbance does not affect the rotor speed controlled by the ISMC-RBF controller, which continues to precisely follow the optimal speed ω_{opt}. The simulation of tracking error $e = \omega_t - \omega_{opt}$, as illustrated in Fig. 7, confirms these observations. The controlled speed provided by ISMC-RBF fluctuates around the optimal speed with the least error, whereas both RBF-NN and ISMC controllers presented higher variations in tracking error.

The results of the electromagnetic torque T_{em} simulation, as depicted in Fig. 8, demonstrate satisfactory performance for both controllers, ISMC-RBF and RBF-NN, with smooth variations observed. To underscore the significance of ISMC-RBF, the STD was considered about the fluctuations of the electromagnetic torque. A lower standard deviation indicates a more stable and consistent torque output from the generator, suggesting that the controller effectively adapts to changing wind conditions and maintains a steady power output. The findings presented in Table 2 indicate that the STD obtained by ISMC-RBF (0.22 kN.m) is lower than that of RBF-NN (0.224 kN.m) and ISMC (0.474 kN.m). Additionally, Table 2 demonstrates that the proposed ISMC-RBF achieves a maximum electromagnetic torque value of only 1.21 kN.m, whereas ISMC reaches 3.88 kN.m. Consequently, the proposed ISMC-RBF controller demonstrates high performance in rejecting fluctuations, thereby minimizing mechanical loads that could potentially cause fatigue.

Electrical power efficiency (η_{el})is a crucial factor to consider, representing the ratio of electrical power output to the available wind power. A higher efficiency value suggests that the controller effectively converts a larger portion of wind energy into usable electrical power. This indicates a well-designed and optimized control system. Referring to the temporal variations depicted in Fig. 9 and the performance results shown in Table 3, it is evident that the proposed ISMC-RBF controller delivers the most stable electrical power among all three considered controllers. The efficiency reaches up to 95%. Consequently, the ISMC-RBF controller enables higher power extraction compared to the reference controllers.

Tables 1, 2, and 3 present the results for wind speeds of 7, 8, and 9 m.s^{-1}, respectively. It is observed from the tables that the performances of all methods decrease with increasing the mean wind speed. However, the proposed ISMC-RBF method consistently outperforms the other two methods across all wind speeds.

5. Conclusion

A new hybrid controller ISMC-RBF was developed in this work. Its performances were compared to those of the classical RBF-NN and ISMC in the low wind speed regime where the control consists of extracting maximum energy from wind. Adding RBF to ISMC enabled to mitigate the main drawback of this last which is known as chattering phenomenon, and exhibited due to the inherent imposed fast dynamics of the controller. Using the RBF-NN to estimate the nonlinear dynamics of the two-mass model of a wind turbine has enabled to enhance the behavior of ISMC controller and succeeded in limiting these perturbations. This was achieved through ensuring Lyapunov like condition of stability of the hybrid controller while the nonlinear part of system dynamics was actualized through a RBF based learning algorithm. The obtained results have shown that the ISMC-RBF gives the best tracking of the reference wind speed. It yields better extraction of the electrical energy while minimizing fluctuations of mechanical loads.

Author Contributions

The two authors have worked together on the theoretical formalism. They have performed the analytic

calculations. The main author E. El Mjabber has performed the numerical simulations. Both A. Khamlichi and E. El Mjabber contributed to the final version of the manuscript.

References

[1] EL MJABBER, E. K., A. EL HAJJAJI, and A. KHAMLICHI. A hybrid adaptive controller based on sliding mode control and rbf neural network for variable speed wind turbine. *Int. Rev. Appl. Sci. Eng.* 2016, vol. 7, no. 2, pp. 61-70. ISSN: 2062-0810. DOI: 10.1556/1848.2016.7.2.1.

[2] ABOLVAFAEI , M., and S. GANJEFAR. Electrical Power and Energy Systems Maximum power extraction from fractional order doubly fed induction generator based wind turbines using homotopy singular perturbation method. Electr. *Power Energy Syst.* 2020,vol. 119, no. December 2019, p. 105889. ISSN 0142-0615. DOI: 10.1016/j.ijepes.2020.105889.

[3] BOUKHEZZAR, B., and H. SIGUERDIDJANE. Comparison between linear and nonlinear control strategies for variable speed wind turbines. *2010, Control Eng. Pract.*, vol. 18, no. 12, pp. 1357–1368. ISSN 0967-0661. DOI: 10.1016/j.conengprac.2010.06.010.

[4] NIE, Y., J. LIU, L. GAO, Y. WU, and Z. LI. Nonlinear rotor kinetic energy control strategy of DFIG-based wind turbine participating in grid frequency regulation. 2023, *Electr. Power Syst. Res.*, vol. 223, p. 109678. ISSN 0378-7796. DOI: 10.1016/J.EPSR.2023.109678.

[5] EL MJABBER, E. K., A. KHAMLICHI, and A. EL HAJJAJI. Nonlinear control of wind turbine in above rated wind speed region. *Pollack Period.* 2021, vol. 17, no. 1, pp. 72–77. ISSN: 1788-1994. DOI: 10.1556/606.2021.00411.

[6] MOHAMMADI, F. , B. MOHAMMADI-IVATLOO, G.GEVORK B, M. H. ALI, W.WEI, , O. ERDINÇ and M. SHIRKHANI. Robust control strategies for microgrids: A Review. *IEEE Syst J.*. 2022, vol. 16, no. 2, pp. 2401–2412. ISSN 1937234. DOI: 10.1109/JSYST.2021.3077213.

[7] EL YAAKOUBI, A., A. BOUZEM, R. EL ALAMI, N. CHAIBI, and O. BENDAOU. Wind turbines dynamics loads alleviation: Overview of the active controls and the corresponding strategies. *Ocean Engineering*, Elsevier. 2023, vol. 278. ISSN 00298018 DOI: 10.1016/j.oceaneng.2023.114070.

[8] BARAMBONES, O. A robust wind turbine control using a neural network based wind speed estimator. *Proc. Int. Jt. 2010, Conf. Neural Networks.* ISBN: 978-1-4244-6918-5. DOI: 10.1109/IJCNN.2010.5596859.

[9] DELAVARI, A. and A. SHARIFI. Adaptive reinforcement learning interval type II fuzzy fractional nonlinear observer and controller for a fuzzy model of a wind turbine. *Eng Appl Artif Intell.* 2023, vol. 123. DOI: 10.1016/j.engappai.2023.106356.

[10] DE CARVALHO, W. C., R. P. BATAGLIOLI, R. A. S. FERNANDES, and D. V COURY. Fuzzy-based approach for power smoothing of a full-converter wind turbine generator using a supercapacitor energy storage. *Electr. Power Syst. Res.*. 2020, vol. 184, no. February, p. 106287. ISSN 0378-7796. DOI: 10.1016/j.epsr.2020.106287.

[11] ASSAREH, E., and M. BIGLARI. A novel approach to capture the maximum power from variable speed wind turbines using PI controller, RBF neural network and GSA evolutionary algorithm. Renew. Sustain. *Energy Rev.*. 2015,, vol. 51, pp. 1023–1037. ISSN 1364-0321. DOI: 10.1016/j.rser.2015.07.034.

[12] ASGHARNIA, A., A. JAMALI, R. SHAHNAZI, and A. MAHERI. Load mitigation of a class of 5-MW wind turbine with RBF neural network based fractional-order PID controller. *ISA Trans.*. 2020, vol. 96, pp. 272–286. ISSN 0019-0578. DOI: 10.1016/j.isatra.2019.07.006.

[13] SARAVANAKUMAR, R. , and D. JENA. Validation of an integral sliding mode control for optimal control of a three blade variable speed variable pitch wind turbine. *Int. J. Electr. Power Energy Syst.*. 2015, vol. 69, pp. 421–429. ISSN 0142-0615. DOI: 10.1016/j.ijepes.2015.01.031.

[14] BEN ZAROUALA, R. O., and E. El Mjabber. Sliding Mode Based Control for a Flexible Wind Turbine. *Energy Procedia.* 2017, vol. 141, pp. 399–404, 2017. ISSN 1876-6102. DOI: 10.1016/j.egypro.2017.11.050.

[15] CHEHAIDIA, S. E., et al. Robust Nonlinear Terminal Integral Sliding Mode Torque Control for Wind Turbines Considering Uncertainties. *IFAC-PapersOnLine. 2022*, vol. 55, no. 12, pp. 228–233, Jan. 2022. ISSN 2405-8963. DOI: 10.1016/J.IFACOL.2022.07.316.

[16] SARAVANAKUMAR, R. , and D. JENA. Validation of an integral sliding mode control for optimal control of a three blade variable speed variable pitch wind turbine. *Int. J. Electr. Power Energy Syst.*. 2015, vol. 69, pp. 421–429. ISSN 0142-0615. DOI: 10.1016/j.ijepes.2015.01.031.

[17] JIANG,D., W. YU, J. WANG, G. ZHONG, and Z. ZHOU. Dynamic Analysis of DFIG Fault Detection and Its Suppression Using Sliding Mode Control. *IEEE J Emerg Sel Top Power Electron.*. 2023, vol. 11, no. 1, pp. 643–656. ISSN 21686785. DOI: 10.1109/JESTPE.2020.3035205.

[18] KELKOUL, B., and A. BOUMEDIENE. Stability analysis and study between classical sliding mode control (SMC) and super twisting algorithm (STA) for doubly fed induction generator (DFIG) under wind turbine. *Energy*. 2021, vol. 214. ISSN 03605442. DOI: 10.1016/j.energy.2020.118871.

[19] YAICHI, I., A. SEMMAH, P. WIRA, AND Y. DJERIRI. Super-twisting sliding mode control of a doubly-fed induction generator based on the SVM Strategy. *Periodica polytechnica Electrical engineering and computer science*. 2019, vol. 63, no. 3, pp. 178–190. ISSN 20645279. DOI: 10.3311/PPee.13726.

[20] CHOJAA, H., A. DEROUICH, S. E. CHEHAIDIA, O. ZAMZOUM, M. TAOUSSI, and H. ELOUATOUAT. Integral sliding mode control for DFIG based WECS with MPPT based on artificial neural network under a real wind profile. *Energy Reports*. 2021, vol. 7, pp. 4809–4824. ISSN 23524847. DOI: 10.1016/j.egyr.2021.07.066.

[21] MIRZAEI, M. J., M. A. HAMIDA, and F. PLESTAN. Neural network-based supertwisting control for floating wind turbine in region III. *IFAC-PapersOnLine*. 2023, pp. 336–341. ISSN 24058963. DOI: 10.1016/j.ifacol.2023.10.1590.

[22] ASGHARNIA, A., A. Jamali, R. Shahnazi, and A. Maheri. Load mitigation of a class of 5-MW wind turbine with RBF neural network based fractional-order PID controller. *ISA Trans.*. 2020, vol. 96, pp. 272–286. ISSN 0019-0578. Doi: 10.1016/j.isatra.2019.07.006.

[23] BOUKHEZZAR, B., and H. SIGUERDIDJANE. Nonlinear control of a variable-speed wind turbine using a two-mass model. *2011, IEEE Trans. Energy Convers.*, vol. 26, no. 1, pp. 149–162. ISSN: 0885-8969. DOI: 10.1109/TEC.2010.2090155.

[24] ABOLVAFAEI , M., and S. GANJEFAR. Maximum power extraction from a wind turbine using second-order fast terminal sliding mode control. *Renew. Energy*. 2019, vol. 139, pp. 1437–1446. ISSN 0960-1481. DOI: 10.1016/j.renene.2019.03.044.

[25] HEMMATI, R., N. AZIZI, M. SHAFIE-KHAH, and J. P. S. CATALÃO. Decentralized frequency-voltage control and stability enhancement of standalone wind turbine-load-battery. *International Journal of Electrical Power and Energy Systems*. 2018, vol. 102, pp. 1–10. ISSN 01420615. DOI: 10.1016/j.ijepes.2018.04.021.

[26] FARZA,M., M. M'SAAD, AND L. ROSSIGNOL. Observer design for a class of MIMO nonlinear systems. *Automatica*. 2004, vol. 40, no. 1, pp. 135–143. ISSN 0005108. DOI: 10.1016/j.automatica.2003.08.008.

[27] RAJENDRAN , S., and D. JENA. Control of Variable Speed Variable Pitch Wind Turbine at Above and Below Rated Wind Speed. *J. Wind Energy*. 2014, vol. 2014, pp. 1–14. DOI: 10.1155/2014/709128.

[28] TAGHINEZHAD, J., and S. SHEIDAEI. Prediction of operating parameters and output power of ducted wind turbine using artificial neural networks. *Energy Reports*. 2022, vol. 8, pp. 3085–3095. ISSN 2352-4847. Doi: 10.1016/J.EGYR.2022.02.065.

[29] LIU, J. Radial Basis Function (RBF) Neural Network Control for Mechanical Systems. *Berlin Heidelberg*, 2013. ISBN: 9783642348167.

About Authors

El Kabira EL MJABBER was born in Morocco, in 1988. She received his M.Sc. degree in microelectronics and industrial computing form University of Sidi Mohamed bn Abdellah in 2013, Morocco. She received Ph.D degree in electronic and automatic from University of Abdelmalek Essaadi in 2020, Morocco. She is currently a professor. Her area of research interest is control of nonlinear systems.

Abdellatif KHAMLICHI was born in Morocco, in 1963. He was graduated as an Engineer form ENTPE in France in 1987. He received Ph.D degree from Ecole Centrale de Lyon in France in 1992. He is now professor at the National School of Applied Sciences in Tetouan. His main research interests are in Mechanics, Mechatronics en Energetic.

Appendix A

- Rotor diameter = 21.65 m
- Air density 1.29 kg.m^{-1}
- Gearbox ratio= 43.165
- Hub height=36.6 m
- Nominal electrical power=600 kW

- Shaft damping coefficient=9500 N.m.rad^{-1}.s^{-1}
- Shaft stiffness coefficient =2.691 105 N.m.rad^{-1}
- Rotor friction coefficient= 27.36 N.m.rad^{-1}.s^{-1}
- Generator friction coefficient=0.2 N.m.rad^{-1}.s^{-1}
- Generator friction coefficient= 0.2 N.m.rad^{-1}.s^{-1}